Geochimica et Cosmochimica Acta 335 (2022) 284–296

Contents lists available at ScienceDirect

Geochimica et Cosmochimica Acta

journal homepage: www.elsevier.com/locate/gca

Bulk compositions of the Chang'E-5 lunar soil: Insights into chemical homogeneity, exotic addition, and origin of landing site basalts

Keqing Zong [a], Zaicong Wang [a,*], Jiawei Li [a], Qi He [a], Yiheng Li [a], Harry Becker [b], Wen Zhang [a], Zhaochu Hu [a], Tao He [a], Kenan Cao [a], Zhenbing She [a], Xiang Wu [a], Long Xiao [a], Yongsheng Liu [a]

[a] State Key Laboratory of Geological Processes and Mineral Resources, School of Earth Sciences, China University of Geosciences, Wuhan 430074, China
[b] Freie Universität Berlin, Institut für Geologische Wissenschaften, Malteserstrasse 74-100, Berlin 12249, Germany

ARTICLE INFO

Article history:
Received 27 January 2022
Accepted 27 June 2022
Available online 30 June 2022
Associate editor: Marc Norman

Keywords:
Chang'E-5
Lunar soil
Clinopyroxene-rich mantle source
KREEP
Meteoritic addition

ABSTRACT

Lunar soil is a fine mixture of local rocks and exotic components. The bulk-rock chemical composition of the newly returned Chang'E-5 (CE-5) lunar soil was studied to understand its chemical homogeneity, exotic additions, and origin of landing site basalts. Concentrations of 48 major and trace elements, including many low-concentration volatile and siderophile elements, of two batches of the scooped CE-5 soil samples were simultaneously obtained by inductively coupled plasma mass spectrometry (ICP-MS) with minimal sample consumption. Their major and trace elemental compositions (except for Ni) are uniform at milligram levels (2–4 mg), matching measured compositions of basaltic glasses and estimates based on mineral modal abundances of basaltic fragments. This result indicates that the exotic highland and KREEP (K, rare earth elements, and P-rich) materials are very low (<5%) and the bulk chemical composition (except for Ni) of the CE-5 soil can be used to represent the underlying mare basalt. The elevated Ni concentrations reflect the addition of about 1 wt% meteoritic materials, which would not influence the other bulk composition except for some highly siderophile trace elements such as Ir. The CE-5 soil, which is overall the same as the underlying basalt in composition, displays low Mg# (34), high FeO (22.7 wt%), intermediate TiO_2 (5.12 wt%), and high Th (5.14 μg/g) concentrations. The composition is distinct from basalts and soils returned by the Apollo and Luna missions, however, the depletion of volatile or siderophile elements such as K, Rb, Mo, and W in their mantle sources is comparable. The incompatible lithophile trace element concentrations (e.g., Ba, Rb, Th, U, Nb, Ta, Zr, Hf, and REE) of the CE-5 basalts are moderately high and their pattern mimics high-K KREEP. The pattern of these trace elements with K, Th, U, Nb, and Ta anomalies of the CE-5 basalts cannot be explained by the partial melting and crystallization of olivine, pyroxene, and plagioclase. Thus, the mantle source of the CE-5 landing site mare basalt could have contained KREEP components, likely as trapped interstitial melts. To reconcile these observations with the initial unradiogenic Sr and radiogenic Nd isotopic compositions of the CE-5 basalts, clinopyroxene characterized by low Rb/Sr and high Sm/Nd ratios could be one of the main minerals in the KREEP-bearing mantle source. Consequently, we propose that the CE-5 landing site mare basalts very likely originated from partial melting of a shallow and clinopyroxene-rich (relative to olivine and orthopyroxene) upper mantle cumulate with a small fraction (about 1–1.5 %) of KREEP-like materials.

1. Introduction

The returned samples from previously unsampled regions in the Moon can allow us to answer many of the outstanding questions in lunar formation and evolution (Yang and Lin, 2021). China's Chang'E-5 (CE-5) mission landed on Dec. 1, 2020, at 43.06°N, 51.92°W within the Procellarum-KREEP Terrane of the Moon and represents the first lunar sample return mission since Apollo (USA) and Luna (Soviet) missions in the 1970s (Li et al., 2022). The landing site is far away from the Apollo and Luna landing sites and sampled a mare plain (designated Em4/P58) in the Northern Oceanus Procellarum where the young lunar mare basalts are exposed on the lunar surface (Che et al., 2021; Hiesinger et al., 2011; Li et al., 2021b; Qian et al., 2021a). The CE-5 mission brought back a total weight of 1731 g of lunar regolith by automated scooping and drilling. The bulk chemical compositions of the new CE-5 lunar soil provide important constraints on various lunar processes.

* Corresponding author.
E-mail address: zaicongwang@cug.edu.cn (Z. Wang).

https://doi.org/10.1016/j.gca.2022.06.037
0016-7037/

Remote telescopic and orbital spectroscopic investigations have provided regional and global views on the bulk chemistry and thus the fundamental element distribution and evolution of the Moon (e.g., Gillis et al., 2004; Lawrence et al., 1998; Lawrence et al., 2002; Prettyman et al., 2006; Qian et al., 2021b). Analysis of the returned lunar soils in the laboratory can serve as the ground truth to calibrate remote sensing data of chemical properties of the lunar surface (Hiesinger and Head, 2006) and allow construction of global chemical maps (Shearer and Borg, 2006; Shearer et al., 2006). The composition of lunar soils is often affected by lateral mixing of impact ejecta (local and/or exotic) and the addition of meteoritic materials (e.g., Head and Wilson, 2020; McKay et al., 1991). Whether or not these processes affected the compositions of the CE-5 soil is not currently clear. The extent to which their compositions differ from returned Apollo and Luna samples are not well understood (Li et al., 2022, Yao et al. 2022). High concentrations of volatiles and heat-producing elements like K, U, and Th that are mainly distributed in the KREEP, a material characterized by K, rare earth elements, and P-rich, in the mantle source are expected to have sustained young mare magmatism in the Northern Oceanus Procellarum (Laneuville et al., 2018). However, Tian et al. (2021) suggested a non-KREEP origin for the CE-5 basalts based on unevolved Sr-Nd isotopic compositions and make us reconsider the thermal evolution of the Moon.

Up to now, work mainly focused on petrology, in-situ mineral chemical compositions, and formation timing of basaltic clasts of the CE-5 regolith (Che et al., 2021; He et al., 2022; Hu et al., 2021; Li et al., 2021b; Tian et al., 2021). Li et al. (2022) and Yao et al. (2022) reported major and some trace element compositions of the CE-5 soils using conventional methods of X-ray fluorescence spectrometry (XRF) and instrumental neutron activation analysis (INAA). However, due to low concentrations, some elements of great interest such as Cu and Mo have not been reported. Moreover, the characteristics and origin of the CE-5 basalts were mainly based on the assumed rare earth elements (REE) of basaltic fragments (He et al., 2022; Tian et al., 2021). Chondrite-normalized patterns of other trace elements and some elemental ratios such as K/U, W/U, Mo/Nd, Nb/Ta, and Zr/Hf that show the highly consistent compatibility during magmatic process also provide important roles in understanding the origin of lunar basalts (Albarede et al., 2015; Münker, 2010; Newsom, 1986; Warren, 1989). A comprehensive bulk chemical composition of the returned CE-5 soils is thus indispensable for understanding the relevant magmatic and thermal evolution of the Moon.

Inductively coupled plasma mass spectrometry (ICP-MS) has been widely used for routine determination of concentrations of many elements in geological samples owing to its excellent detection limit and sensitivity, low sample consumption, and simple preparation procedure (e.g., Ammann, 2007; Longerich et al., 1990). Importantly, with a suitable analytical strategy, this technique can yield accurate concentrations of major and trace elements determined simultaneously from the same sample aliquot. In this study, 48 major and trace elements of two batches of the scooped CE-5 lunar soils (CE5C0400 and CE5C0600) were determined by ICP-MS for seven replicates at a few-milligram level. Sample homogeneity and effects of exotic addition by impact ejecta and meteorites are evaluated. We further compare the CE-5 chemical compositions with compositions determined by remote sensing methods and with lunar samples returned by the Apollo and Luna missions. Based on the new bulk compositions, we also propose the KREEP-bearing, clinopyroxene-rich mantle origin of the CE-5 basalts which resulted in low melting liquidus and KREEP-like trace element compositions.

2. Materials and methods

2.1. Major and trace elemental analyses of the CE-5 soils by ICP-MS

Two batches (200 mg CE5C0400 and 400 mg CE5C0600) of the scooped CE-5 lunar soils that were not sieved during sampling and preparation, were obtained from the China National Space Administration Agency. Their bulk chemical compositions were analyzed in this study at the State Key Laboratory of Geological Processes and Mineral Resources, China University of Geosciences, Wuhan (GPMR-Wuhan). To evaluate sample heterogeneity, these two batches of the CE-5 lunar soils were digested by seven replicates in three times with minimal sample consumption (~2 or ~ 4 mg). A lunar soil simulant CUG-1B, basaltic reference materials BCR-2 and BHVO-2, and a lunar meteorite NWA 6950 were manually processed to be smaller particle sizes and used as monitor standards, and they were prepared and analyzed with the CE-5 lunar soil via the same procedure.

Commercially available nitric acid (68% v/v, GR grade) and hydrofluoric acid (40% v/v, GR grade) were distilled twice in a DST-1000 acid purification system (Savillex, USA) and then used in the sample digestion process. Ultra-pure water (18.2 MΩ cm^{-1}) acquired from a Milli-Q water purification system (Millipore, Bedford, MA, USA) was used in all procedures. Standard solutions (1, 10, 25 and 50 ng ml^{-1} for trace elements and 10, 100, 500, 1000 ng ml^{-1} for major elements) used for instrumental calibration curves were prepared by gravimetric serial dilution from 10 μg ml^{-1} multi-element standard solutions (SPEX CertiPrep, NJ, USA) using 2% v/v HNO_3 and 0.05% v/v HF solution. The quality control (QC) solution is a mixture solution of three digested international geological standards of BCR-2, BHVO-2, and RGM-2 with a fixed proportion of 4:3:3 and was used for time-drift correction and long-term quality control. The internal standard solution of indium was diluted from a 1000 μg ml^{-1} single-element standard solution (National Center for Analysis and Testing of Steel Materials, Beijing, China). All acid and solutions were transferred and stored in clean Teflon containers to avoid potential contaminations.

The sample digestion and measurement procedures have been described before by Li et al. (2021a). In this study, small volume (5 ml) Teflon bombs were customized to obtain a better digestion effect for minimal sample weight. The detailed sample digestion procedures were optimized as follows. (1) All samples were weighed and placed into the Teflon bombs and dissolved by 1 ml concentrated HF-HNO_3 mixture (1:1). (2) The bomb was inserted in a special stainless-steel container tightly, then this set was sealed and heated at 190 °C in an electric oven for 48 h. (3) After cooling, the bomb was opened and placed on a hotplate at 120 °C and evaporated to dryness. (4) Then 0.5 ml HNO_3 was added and the sample was evaporated to a second-round dryness. (5) 0.5 ml HNO_3, 0.5 ml ultra-pure water, and a suitable amount of indium solution were added and the residue was re-dissolved. (6) The bomb was assembled and heated at 190 °C in an electric oven for 12 h. (7) After cooling, the sample solution was further evaporated at 120 °C to dryness, then 2% v/v HNO_3 solution was used to dilute the digested samples by a factor of 1000 for ICP-MS measurement.

An Agilent 7700x ICP-MS (Agilent Technologies) was used for all major and trace element measurements. The instrumental parameters were optimized to acquire appropriate signal intensities and stabilities of ^{7}Li, ^{89}Y, and ^{205}Tl. CeO^+/Ce^+ and Ce^{2+}/Ce^+ ratios were monitored and optimized to keep oxide and double-charged ion productions lower than 0.5% and 1.5%, respectively. The background of the instrument was checked after each sample determination. The detailed operating conditions and acquisition parameters of ICP-MS are summarized in Table S1.

Elemental concentrations were calculated through a combination of single internal standardization (In) and multiple external standard calibration methods (Li et al., 2021a). The initial concentrations were calculated online according to the standard calibration curves of the instrument. The correlation coefficient of the standard calibration curve for each element was better than 0.9998. A software ICPMSDataCal (Liu et al., 2010; Zhao et al., 2019) was further used for off-line multiple external standard calibration, oxide interference, and time drift corrections to obtain the final elemental concentrations. The oxide interference correction of Sc and REE followed the routine method of Zhao et al. (2019).

Importantly, lunar basaltic samples are characterized by higher Ti concentrations than terrestrial basalts, which would cause strong oxide interference on Cu. A single-element standard solution of Ti was thus prepared to measure the oxide production rate of Ti and then used to conduct the oxide interference correction on Cu. Although Ti-Ar polyatomic ion has potential interference on Zr, the production rate of the interference $^{50}Ti^{40}Ar$ for our instrument is very low (0.002%), which indicates negligible Ti-Ar interference on Zr. Lead is a volatile element that was almost completely lost during the early accretion and formation of the Moon. The process led to very low common ^{204}Pb and high radiogenic ^{206}Pb, ^{207}Pb, and ^{208}Pb in lunar samples. Therefore, ^{206}Pb, ^{207}Pb, and ^{208}Pb were determined together to recalculate the total Pb concentration of lunar samples. Due to the loss of Si during the sample digestion process and the anhydrous feature of the lunar sample, SiO_2 concentration was obtained by subtraction of other major elements from 100 wt%. The results of monitor standards of BHVO-2, BCR-2, CUG-1B, and NWA 6950 are listed in Table S2 and Figure S1. They show the relative errors better than 5% and 10% for most major and trace elements, respectively, except for Mo and W with high uncertainty (20–40%) due to low concentrations.

2.2. Major elemental analysis and image of metals in the CE-5 agglutinates

The back-scattered electronic (BSE) image of the CE-5 agglutinates was obtained by scanning electron microscopes (FE-SEM, FEI Quanta 200) equipped with energy dispersive spectrometers (EDS) at the GPMR-Wuhan. Major elemental compositions of metals in the CE-5 agglutinates were determined using a JEOL JXA-8230 electron microprobe analyzer (EPMA) at the GPMR-Wuhan. Minerals were analyzed using 15 kV accelerating voltage and a 20 nA focused beam (1 μm diameter). Natural mineral and glass standards were used with ZAF matrix correction.

3. Results

The concentrations of two batches of the CE-5 lunar soils (CE5C0400 and CE5C0600), including seven replicates and their weighted mean, are listed in Table 1 and shown in Fig. 1. Major and trace elemental compositions of seven replicates are consistent with each other within 10% relative standard deviations (RSDs), except for a few elements that mostly show low concentrations (e.g., Mo and W) and one replicate with high Ni concentration (Fig. 1a). However, we note a small systematic analytical error in these data and if all the data are normalized to a constant FeO concentration, the RSDs are almost smaller than 5% (Fig. 1b). Therefore, the CE-5 lunar soil is uniform at the milligram level and consequently, the weighted mean values based on the consumed 18.21 mg materials of the present study likely represent the bulk chemical composition of the CE-5 lunar soil, scooped at the landing site. Most trace elemental concentrations of the CE-5 soils obtained by ICP-MS in this study agree with the INAA results reported by Li et al. (2022) and Yao et al. (2022), except for Rb, Cs, Tm, and W with low concentrations (Fig. 1). Importantly, major and trace elemental concentrations (except for Ni) of the CE-5 lunar soils are consistent in the uncertainty with the measured results of basaltic glasses (He et al., 2022) and reconstructed results of basaltic fragments (Che et al., 2021; He et al., 2022; Tian et al., 2021) (Figs. 2 and 3). Overall, the CE-5 lunar soils, the same as the underlying mare basalts, are characterized by intermediate TiO_2 (5.12 wt%), high FeO (22.7 wt%) and Th (5.14 μg/g), and low MgO (6.52 wt%) and Mg# (34), which are different from the Apollo and Luna soils and basalts (Table 1 and Figs. 2 and 4). However, the concentration of Ni (139 μg/g) in the CE-5 soils is obviously high for a lunar basalt or meteorite at the same Mg# (Fig. 5a) and basaltic fragments (34 ± 48 μg/g) of the CE-5 (He et al., 2022). Numerous small and round Fe-Ni metal alloys were found in the agglutinates from the CE-5 soils (Fig. 5b), which are characterized by the high Ni (5.3–6.26 wt%) and Co (0.43–0.51 wt%) concentrations and the high Ni/Co ratios of 11.2–14.6 (Table S3).

Both the CE-5 soils and basalts show the same CI-chondrite normalized REE and multiple-element patterns (Fig. 6a, b), which are different from the Apollo low-Ti and high-Ti basalts, especially in the low-Ti basalt normalized multiple-element patterns (Fig. 6c). Europium is depleted in the CI-chondrite normalized REE pattern with Eu/Eu^* and La/Sm values of 0.46 and 2.1, respectively (Table 1 and Fig. 6a). Incompatible lithophile elements of Ba, Rb, Th, REE, Nb, Ta, Zr, and Hf have very high concentrations in the CE-5 basalts/soils relative to the Apollo high-Ti and low-Ti basalts, and they show negative anomalies of Cs, Rb, K, Sr, P, and Eu in the CI-chondrite normalized multiple-element pattern (Fig. 6b). The CE-5 basalts/soils show K/U, Rb/Ba, W/U, and Mo/Nd ratios of 1276, 0.013, 0.37, and 0.00055, respectively, which is comparable with other mare basalts (Fig. 7). The Nb/Ta and Zr/Hf ratios of the CE-5 basalts/soils are 19.5 and 38.9, respectively, which is similar to the KREEP-related samples but different from the Apollo low-Ti and high-Ti basalts (Fig. 8).

4. Discussion

4.1. Homogeneity of the CE-5 lunar soil and ground-truth calibration of remote spectroscopic data

Our result demonstrates that the chemical composition (except for Ni) of the CE-5 lunar soil is remarkably uniform even at 2 mg level (Fig. 1). Overall, the new values overlap the most measurements by Li et al. (2022) and Yao et al. (2022) via different analytical techniques (XRF and INAA) and for ~ 200 mg of other sample batch, except for low-concentration Na and P using XRF and Rb, Cs, Tm, and W using INAA (Fig. 1). Geological and other reference materials such as NWA 6950, CUG-1B, BCR-2, and BHVO-2 also show identical compositions at 2 or 4 mg levels (Table S2 and Fig. S1) because their particle size distributions display a range similar to that of the CE-5 soil (mostly several μm, Fig. S2). Li et al. (2022) examined 155 mg scooped CE-5 soil for its particle size distribution and indicated that up to 95 % of the particle sizes are <10 μm, which is the same as our results obtained by a Raman-based particle analysis system (Cao et al., 2022) (Fig. S2a). Moreover, 95% of the CE-5 soil by mass is distributed in the size of 4.84–432.3 μm (Li et al. 2022). The composition homogeneity of the CE-5 lunar soil thus can be ascribed to the very fine particle sizes, indicating high soil maturity (McKay et al., 1974).

Given the homogeneity, the bulk-rock chemical compositions are therefore suitable for ground-truth calibration of remote spectroscopic data. Remote spectroscopic investigations have been widely applied for global maps of compositional distribution (e.g., Lawrence et al., 1998; Prettyman et al., 2006). Concentrations of TiO_2, Th, K, and FeO are particularly interesting, e.g., TiO_2 is used

Table 1
Major and trace element concentrations of two batches of the scooped Chang'E-5 soils.

Elements	unit	CE5C0400 batch				CE5C0600 batch			Weighted Mean	1SD
		2.05 mg	2.04 mg	1.98 mg	4.13 mg	2.00 mg	2.03 mg	3.98 mg		
SiO_2*	wt.%	43.25	40.85	38.43	40.70	42.08	42.03	41.61	41.25	1.52
MgO	wt.%	6.31	6.53	7.07	6.59	6.50	6.71	6.18	6.52	0.29
Al_2O_3	wt.%	11.19	11.70	11.86	11.62	11.61	11.35	11.49	11.55	0.22
CaO	wt.%	11.08	11.86	11.96	11.49	11.66	11.49	11.86	11.64	0.30
TiO_2	wt.%	5.11	5.30	5.08	5.17	4.86	5.26	5.09	5.12	0.14
FeO	wt.%	21.9	22.5	24.3	23.2	22.1	22.0	22.6	22.7	0.9
Na_2O	wt.%	0.45	0.46	0.47	0.46	0.46	0.47	0.46	0.46	0.01
Na	μg/g	3346	3402	3518	3406	3432	3455	3410	3421	53
K_2O	wt.%	0.20	0.21	0.22	0.22	0.19	0.20	0.20	0.21	0.01
K	μg/g	1656	1736	1791	1866	1617	1688	1665	1728	87
MnO	wt.%	0.27	0.28	0.30	0.28	0.27	0.27	0.28	0.28	0.01
Mn	μg/g	2077	2205	2297	2183	2071	2074	2149	2154	85
P_2O_5	wt.%	0.26	0.28	0.30	0.29	0.25	0.25	0.26	0.27	0.02
P	μg/g	1121	1224	1296	1256	1086	1082	1154	1181	85
Li	μg/g	14.8	15.6	15.7	16.2	14.5	15.5	14.9	15.4	0.6
Be	μg/g	2.76	2.82	3.00	2.95	2.67	2.78	2.82	2.84	0.11
Sc	μg/g	60.3	65.3	64.6	62.6	60.9	62.3	63.9	62.9	1.8
V	μg/g	82.6	93.3	94.1	88.7	95.4	95.2	97.2	92.5	5.1
Cr	μg/g	1367	1401	1570	1378	1593	1422	1513	1459	94
Co	μg/g	37.2	36.1	38.3	37.2	36.4	37.1	37.8	37.2	0.8
Ni	μg/g	167	130	141	135	142	135	131	139	13
Cu	μg/g	12.2	12.4	13.0	13.5	10.9	10.7	11.7	12.2	1.1
Zn	μg/g	14.2	14.0	13.6	14.5	14.7	13.7	14.1	14.2	0.4
Ga	μg/g	5.45	5.79	5.83	5.76	5.74	5.64	6.09	5.79	0.19
Rb	μg/g	4.87	5.08	5.35	5.75	4.98	5.04	5.10	5.23	0.30
Sr	μg/g	305	323	322	310	314	299	318	313	9
Y	μg/g	107	116	123	122	109	114	116	116	6
Zr	μg/g	514	542	574	567	511	523	554	545	25
Nb	μg/g	34.2	35.6	36.9	38.0	32.4	33.8	35.7	35.6	1.9
Mo#	μg/g	0.031	0.031	0.029	0.026	0.035	0.041	0.038	0.033	0.005
Cs	μg/g	0.21	0.22	0.23	0.22	0.20	0.20	0.21	0.22	0.01
Ba	μg/g	364	399	409	424	369	369	399	395	23
La	μg/g	33.2	36.5	38.2	36.6	33.0	33.7	35.2	35.4	2.0
Ce	μg/g	92.6	100	106	103	91.3	93.8	98.8	98.6	5.5
Pr	μg/g	11.8	13.0	13.8	13.2	11.7	12.1	12.6	12.7	0.8
Nd	μg/g	56.2	61.3	64.1	61.9	54.9	56.0	58.9	59.3	3.5
Sm	μg/g	15.8	17.1	18.1	17.6	15.8	16.5	17.3	17.0	0.9
Eu	μg/g	2.65	2.84	2.84	2.82	2.72	2.61	2.82	2.77	0.10
Gd	μg/g	18.3	19.9	20.9	20.2	18.1	19.0	19.7	19.6	1.0
Tb	μg/g	3.04	3.30	3.49	3.42	3.03	3.17	3.30	3.27	0.18
Dy	μg/g	19.1	20.8	21.9	21.4	18.9	20.0	20.5	20.5	1.1
Ho	μg/g	3.83	4.14	4.37	4.30	3.78	3.91	4.01	4.07	0.23
Er	μg/g	10.6	11.6	12.0	11.9	10.6	11.0	11.1	11.3	0.6
Tm	μg/g	1.46	1.58	1.73	1.61	1.46	1.52	1.58	1.57	0.09
Yb	μg/g	9.39	9.95	10.3	10.2	9.34	9.76	10.0	9.90	0.38
Lu	μg/g	1.28	1.38	1.44	1.43	1.25	1.33	1.35	1.36	0.07
Hf	μg/g	13.8	14.5	14.0	15.0	12.6	13.0	14.0	14.0	0.8
Ta	μg/g	1.81	1.84	1.88	1.85	1.68	1.80	1.85	1.83	0.07
W#	μg/g	0.47	0.47	0.57	0.41	0.54	0.61	0.51	0.50	0.07
Pb$	μg/g	1.93	1.97	1.97	1.89	1.96	1.69	1.84	1.89	0.10
Th	μg/g	4.81	5.14	5.51	5.40	4.77	4.99	5.11	5.14	0.28
U	μg/g	1.27	1.39	1.42	1.44	1.22	1.32	1.35	1.35	0.08

* SiO_2 content was calculated by subtraction of other major elements from 100 wt%.
# High uncertainty (20–40%) due to low concentrations.
$ ^{206}Pb, ^{207}Pb, and ^{208}Pb were determined together to recalculate the total Pb content of lunar samples.

for classifying lunar basalts (Neal and Taylor, 1992) and Th-K for identifying the distribution of the KREEP component and heat-producing elements (Laneuville et al., 2018). Fu et al. (2021) and Qian et al. (2021a) predicted the mean FeO concentration in the CE-5 landing region to be between 19.2 wt% and 17 wt%, respectively, both of which are lower than our new value (FeO = 22.7 wt %, Fig. 4 and Table 1). In contrast, the Th concentration (5.14 μg/g) in the CE-5 lunar soil determined in the laboratory is about 20% lower than the value of 6.2 μg/g predicted by Fu et al. (2021) from remote sensing data (Fig. 4). Moreover, our TiO_2 result (5.12 wt%) is also at the lower end-member of the range of 5–8 wt% predicted from remote sensing data (Qian et al., 2021a; Qian et al., 2021b). The remote sensing data show a unimodal distribution of TiO_2 concentrations most frequently in the Oceanus Procellarum region (Qian et al., 2021a). They are very different from returned Apollo and Luna basalt samples and lunar meteorites which display bimodal distributions of low-Ti and high-Ti basalts and rarely intermediate TiO_2 concentrations (Giguere et al., 2000; Gillis et al., 2003). In summary, FeO concentration in the CE-5 lunar soil determined in the laboratory is higher by 20–30%, compared to remote spectroscopic results, whereas Th and Ti concentrations are systematically lower by < 20%. Generally, our data matches well with the remote sensing data. For the Em4/P58 unit, there are some internal composition variations captured by the Clementine TiO_2 and FeO data, mostly related to the impact rays (Qian et al., 2021b). There may also be some variations that cannot be captured by the remote

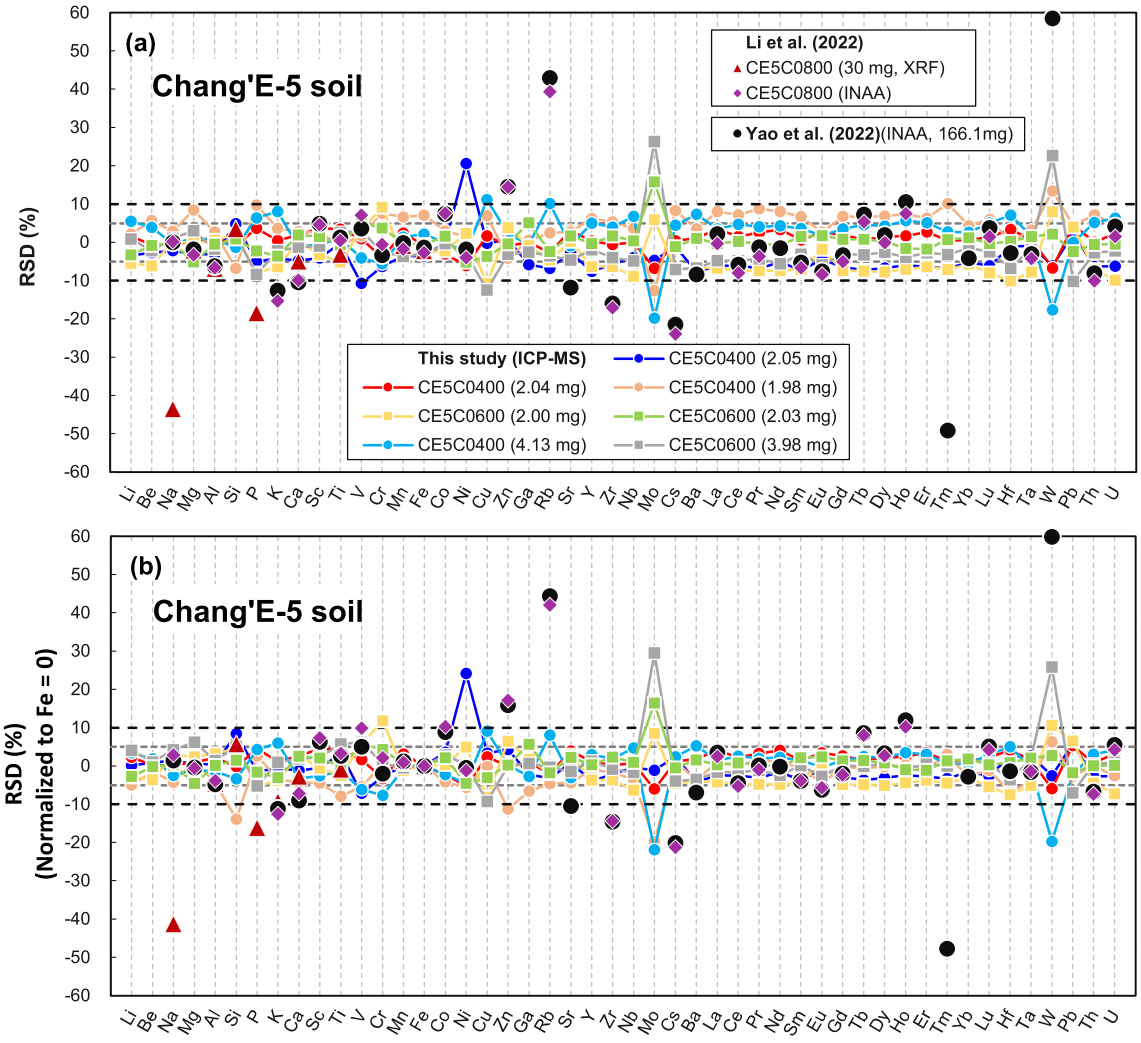

Fig. 1. (a) Relative standard deviations (RSD) of 48 major and trace elements from seven replicates analyzed by ICP-MS of two batches (CE5C0400 and CE5C0600) of the scooped CE-5 soils at ~ 2 mg and ~ 4 mg consumptions. (b) All the data are normalized to a constant FeO concentration given a small systematic analytical error in Fig. 1a. The result shows that the CE-5 soils are remarkably uniform at milligram levels, except for Mo and W with low concentrations and one replicate with high Ni content. The results from 30 mg by XRF (Li et al., 2022) and 166.1 mg by INAA (Yao et al., 2022) are shown for comparison.

sensing in their resolution (~300 m/pixel) that are deduced by local small impacts. For the Th data, its resolution is very low (0.5°/pixel) and such a signature is a mixture of a large area (Fu et al., 2021). Our data can represent the landing site but not the entire Em4/P58 unit. In addition, the detection depth of the remote sensing technique is usually < 1 μm, which is more easily accumulated lunar dust from other units. But the CE-5 scooped samples are obtained from a depth of ~ 3 cm, which may represent the CE-5 basalts much well than the remote sensing data. Although the specific origin of these discrepancies remains to be evaluated, our results confirm the presence of intermediate-Ti, high-FeO, and high-Th basalts in the Em4/P58 region and thus support its wide distribution in the Procellarum-KREEP Terrain as indicated by remote sensing data (Giguere et al., 2000; Gillis et al., 2003; Jolliff et al., 2000).

4.2. Effects of exotic impact ejecta and meteoritic materials

The mixture of local and distant ejecta materials, as well as meteoritic materials, are very common in lunar surface samples, e.g., they are always found in the Apollo soils (e.g., Korotev and Gillis, 2001; Korotev et al., 2011; McKenzie and O'nions, 1991). Previous remote sensing investigations inferred that the CE-5 landing region was contaminated by ejected materials from impact craters but different studies suggest variable proportions of exotic, non-mare components from < 10 % to up to 40% (e.g., Fu et al., 2021; Liu et al., 2021; Qian et al., 2021a; Xie et al., 2020). Importantly, the major and trace elemental concentrations (except for Ni) in soil samples measured in this study overlap compositions of the basaltic glasses and estimates based on mineral modal abundances of the basaltic fragments that show no obvious shock effects (CE5-B1 in Che et al., 2021; He et al., 2022; Tian et al., 2021) (Figs. 2 and 3). For example, our lunar soil and basaltic fragments consistently display high FeO concentrations of 22.15–22.7 wt%. Moreover, trace elemental concentrations (except for Ni) also match each other within analytical uncertainty (Fig. 3b). Such consistency between the CE-5 fine soils (95% of the soil by mass is distributed in the size of 4.84–432.3 μm, Li et al., 2022) and large basaltic fragments (several mm) confirms the limited contamination with exotic ejected materials from other localities of the Moon. Otherwise, the previously proposed significant contamination with KREEP-rich or highland plagioclase-rich distal ejecta (Fu et al., 2021; Liu et al., 2021) would noticeably change major elements and trace element compositions because such

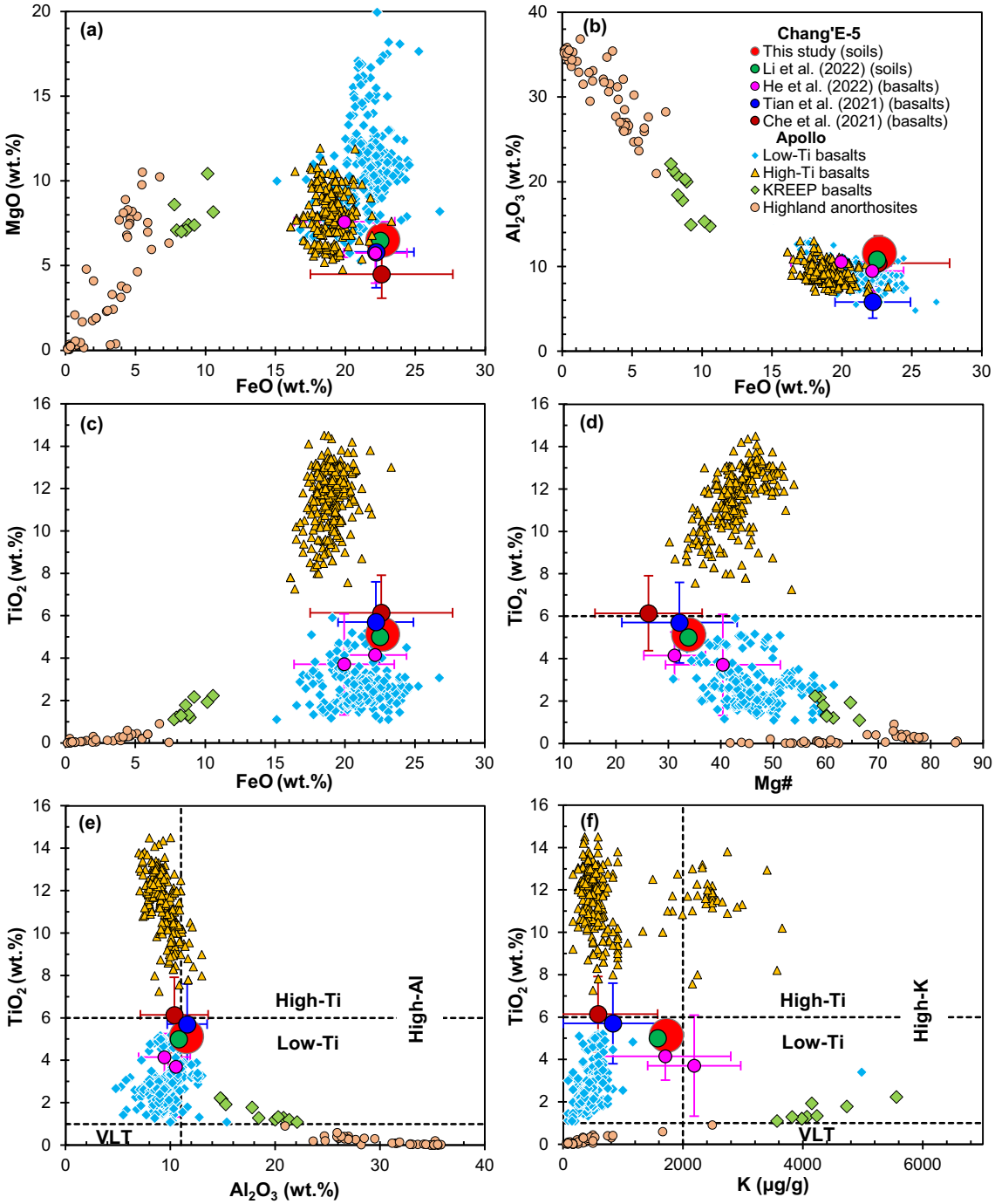

Fig. 2. Major element constituents of the CE-5 soils and comparison with the CE-5 basalts represented by the basaltic glasses (He et al., 2022) and fragments (Che et al., 2021; He et al., 2022; Tian et al., 2021). The classification of the lunar mare basalts is based on the scheme of Neal and Taylor (1992). Note that the results measured from the bulk soils (this study and Li et al., 2022) overall match the estimated compositions from basaltic glasses (He et al., 2022) and large basaltic fragments (Che et al., 2021; He et al., 2022; Tian et al., 2021). The data of lunar low-Ti (Apollo 12&15), high-Ti (Apollo 11&17), and KREEP basalts (Apollo 14&15) and highland anorthosites (Apollo 16) are from The Lunar Sample Compendium (https://www-curator.jsc.nasa.gov/lunar/lsc/index.cfm).

materials show very different compositions from the CE-5 basalts (Figs. 2, 4 and 6). In comparison with CE-5 and Apollo basalts, the highland anorthosites have the highest Al_2O_3 and the lowest FeO contents (Fig. 2b), while KREEP contains the highest Th and U contents (Figs. 4 and 6). Therefore, we can use major elements of Al_2O_3 and FeO and trace elements of Th and U to quantify the addition of the highland and KREEP materials in the CE-5 soils (Fig. S3). Our calculated results show that the exotic additions of the highland and KREEP materials are less than 3% and 5%, respectively (Fig. S3), which would not cause the chemical discrepancy between the CE-5 soils and the underlying basalts in the analytical uncertainty (Figs. 2, 3 and 6). Furthermore, contamination with distal ejecta likely would also induce considerable compositional heterogeneity among soil samples, which is not observed (except for Ni) (Fig. 1). Thus, the laboratory-based measurements (this study, Li et al., 2022, and Yao et al., 2022) are consistent with the prediction that the CE-5 soil predominantly resulted from the local mare basalts and is essentially free of contamination (<5%) by exotic ejected highland and KREEP materials. This result also reconciles with the data of remote sensing (Qian et al., 2021b).

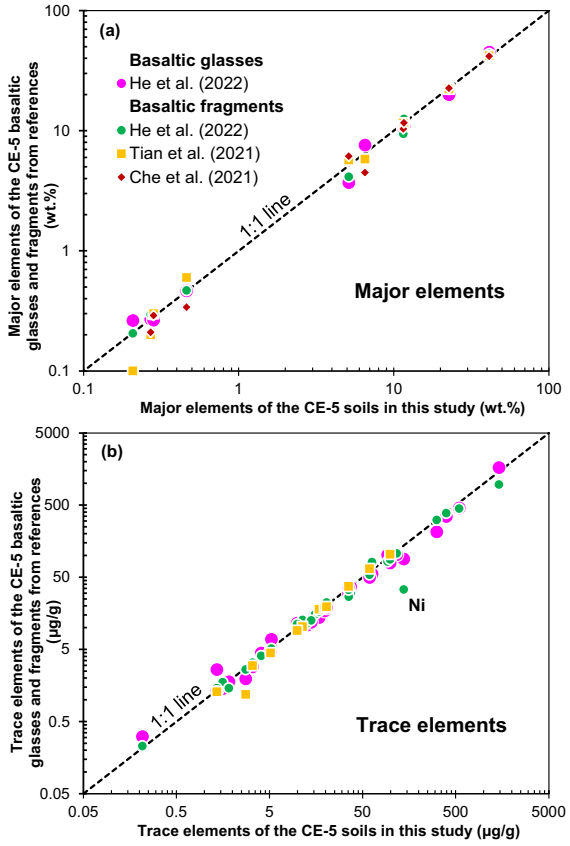

Fig. 3. Comparison of the bulk composition of the CE-5 soils (this study) with the measured average major element (a) and trace element (b) compositions of the CE-5 basaltic glasses (He et al., 2022) and estimated average results from the CE-5 basaltic fragments (Che et al., 2021; He et al., 2022; Tian et al., 2021).

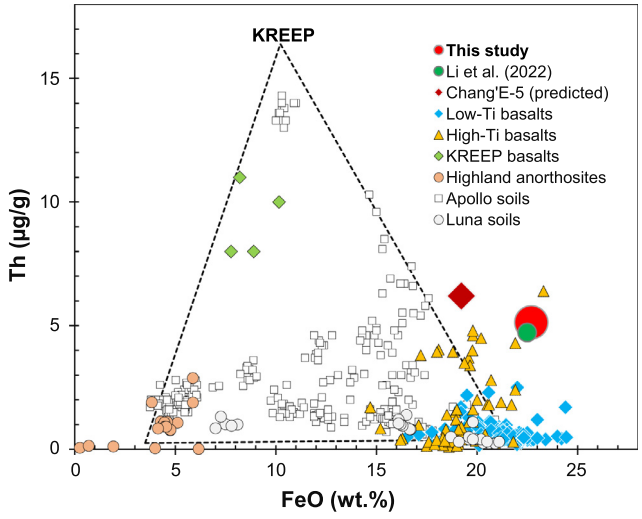

Fig. 4. FeO and Th concentrations of the CE-5 soils. The predicted (Fu et al., 2021) and measured (Li et al., 2022) results are shown for comparison. The measured results (this study and Li et al., 2022) are approximately consistent with the predicted range by remote sensing data (Fu et al., 2021). The data of lunar low-Ti (Apollo 12&15), high-Ti (Apollo 11&17), and KREEP basalts (Apollo 14&15), highland anorthosites (Apollo 16), and Apollo and Luna soils are from The Lunar Sample Compendium (https://www-curator.jsc.nasa.gov/lunar/lsc/index.cfm).

Micrometeorite impacts are ubiquitous on the lunar surface and lead to the strong comminution of local rocks (e.g., Anders et al., 1973; Head and Wilson, 2020; Fischer-Gödde and Becker, 2012; Keays et al., 1970; McKay et al., 1991; Norman et al., 2002; Wasson et al., 1975). The basalt sampled by the CE-5 soil is a highly evolved magmatic product as indicated by the low Mg# of 34 (Fig. 2d). Nickel is essentially incorporated into early crystalizing olivine and pyroxene due to the high partition coefficients of 8.5–47 (Adam and Green, 2006) and its concentration would dramatically decrease particularly at advanced stages of fractional crystallization. Based on available lunar basalt data, the CE-5 basalt would be expected from its Mg# of 34 to contain about 20–30 μg/g Ni (Fig. 5a). However, the bulk Ni concentration of the soil from this study, Li et al. (2022), and Yao et al. (2022) is consistently around 140 μg/g. The Ni excess of ~ 110–120 μg/g must reflect the addition of meteoritic materials to the bulk soil. High Ni/Co ratios (11.2–14.6) of rounded blebs of Fe-Ni metal in the agglutinates is consistent with this interpretation (Day, 2020) (Table S3 and Fig. 5b).

The proportion of meteoritic materials in lunar soil can be estimated by comparing the elevated concentrations of siderophile elements such as Ni, Ir, and Pt to their concentrations in typical chondritic materials (Anders et al., 1973; Haskin and Warren, 1991; Keays et al., 1970; McKay et al., 1991; Wasson et al., 1975). Different groups of chondrites display high Ni concentrations of 1–1.7 wt% (Wasson and Kallemeyn, 1988), indicating about 1 wt% addition of chondrite materials to account for the excess of ~ 110–120 μg/g Ni in the CE-5 soils. Moreover, the CE-5 soil has an Ir concentration of 3.61 ng/g (Yao et al., 2022), which is higher than that in the lunar mare basalts of 0.001–0.04 ng/g (Day et al., 2007). Different groups of chondrites show high Ir concentrations of 360–760 ng/g (Wasson and Kallemeyn, 1988), which also suggests the addition of 0.5–1 wt% of chondrite materials to the CE-5 soils. Therefore, we can conclude that about 1 wt% of meteoritic materials were added to the CE-5 lunar soil. The proportion could be less if iron meteorites were partly involved given their higher Ni and Ir concentrations (Scott and Wasson, 1975). However, the Apollo mature soils have about 1.5–2 wt% addition of chondrite meteorites (Anders et al., 1973; Ganapathy et al., 1970; Haskin and Warren, 1991; Keays et al., 1970; Wasson et al., 1975), which is relatively higher than about 1 wt% addition of chondrite meteorites in the CE-5 soils. If we considered the younger eruption age (2.0 Ga) of the CE-5 basalts (Che et al., 2021; Li et al., 2021b) than the Apollo basalts of 3.1–3.9 Ga (Snape et al., 2019), the average meteoritic influx rate recorded by the lunar soils seems to be similar for the Moon after late heavy bombardment event (3.9 Ga) (Bottke and Norman, 2017). However, based on the data on chondrites (Wasson and Kallemeyn, 1988), mass balance calculation suggests that such addition would not noticeably elevate the concentrations of Fe, Mo, and W, and most other elements in the bulk CE-5 lunar soil. One replicate of this study shows an elevated Ni concentration of 167 μg/g (Fig. 1), likely reflecting the heterogeneous distribution of added meteoritic materials at the milligram sample level.

4.3. KREEP-bearing mantle source of the CE-5 basalts

As discussed above, except for about 1 wt% addition of chondritic meteorites in the CE-5 soils which have elevated some siderophile elements such as Ni and Ir, the exotic highland and KREEP materials can be limited (<5%) and the bulk chemical compositions of the CE-5 soils in this study (except for Ni) thus represent the underlying mare basalts in the analytical uncertainty (Figs. 2-3 and 6). Therefore, we can use the major and incompatible lithophile trace elemental compositions of the CE-5 soils to constrain the mantle source of the CE-5 landing site basalts as below.

The TiO_2, Al_2O_3, and K concentrations are fundamental for classifying lunar basalts (Neal and Taylor, 1992). The CE-5 lunar basalt compositions indicate low-intermediate Ti (<6 wt% TiO_2), high-Al (>11 wt% Al_2O_3), and low-K (<2000 μg/g) basaltic compositions

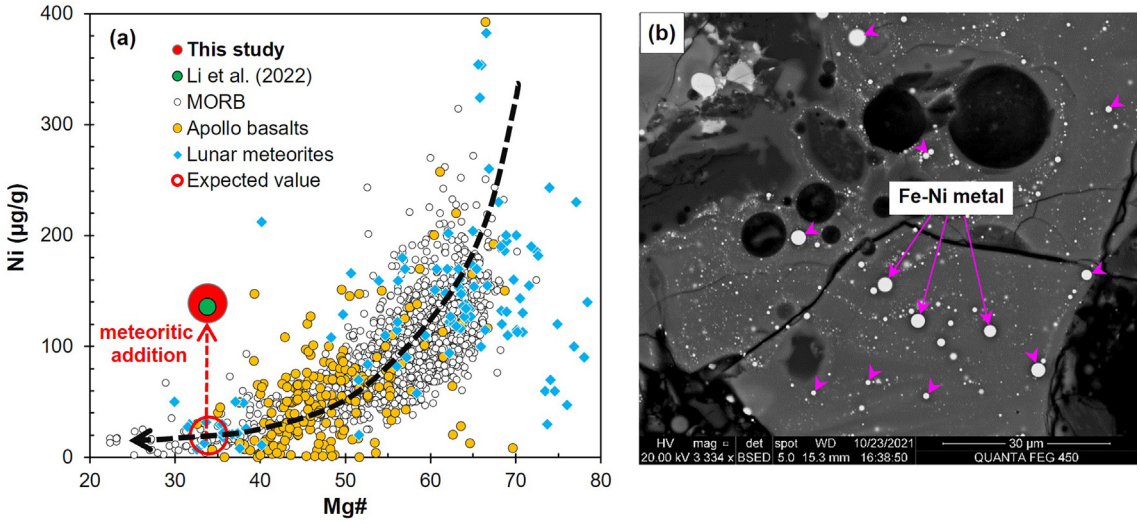

Fig. 5. (a) Covariation of Mg# with Ni concentrations of the CE-5 soils. The elevation of measured Ni concentration relative to Mg# reflects the addition of meteoritic materials. (b) Occurrence of numerous small and round Fe-Ni metal alloys with the high Ni/Cr ratios (11.2–14.6) in an agglutinate from the CE-5 soils. The data of Apollo basalts and lunar meteorites are from The Lunar Sample Compendium (https://www-curator.jsc.nasa.gov/lunar/lsc/index.cfm). The data of terrestrial mid-ocean ridge basalts (MORB) are from Gale et al. (2013).

(Fig. 2). Characteristic, and very different from most mare basalts are the high FeO (22.7 wt%), low MgO (6.52 wt%) concentrations, and low Mg# of 34 (Fig. 2). Such a feature could result from a high degree fractional crystallization. The negative anomalies of Sr and Eu in lunar basalts reflect the effect of the early-stage formation of plagioclase-rich lunar crust from the lunar magma ocean (e.g., Elkins-Tanton et al., 2011; Shearer and Papike, 1999; Warren, 1985). The K/U and Rb/Ba ratios of the CE-5 basalts are within the range of ratios shown by other lunar basalts (Fig. 7a-b). A similar observation can be made for siderophile incompatible trace elements such as W and Mo because the W/U and Mo/Nd ratios in the CE-5 basalts are very low and at a level similar to other lunar basalts (Fig. 7c-d). Consequently, in the first order, the depletion of volatile and siderophile elements in all lunar basalts of different ages and locations (Apollo, Luna, and CE missions) reflects that all lunar mantle sources sampled so far record the effects of lunar core formation (as indicated by low concentrations of Mo and W and low Mo/Nd and W/U) and large-scale volatilization (low K/U and Rb/Ba of the lunar mantle) associated with the lunar magma ocean or lunar formation (Albarede et al., 2015; Newsom, 1986).

The CE-5 lunar basalt was collected from the Procellarum-KREEP Terrane and the concentrations of incompatible lithophile trace elements (e.g., Ba, Rb, Th, U, Nb, Ta, Zr, Hf, and REE) are high and only lower than that of high-K KREEP by a factor of around 3, suggesting a KREEP-like signature of the CE-5 basalt (Fig. 6c), which is also observed in the study of Tian et al. (2021) based on the reconstructed REE patterns.

The CE-5 basalt formed from high degree fractionation of a low-Ti primary basaltic magma (e.g., He et al 2022; Tian et al 2021; Zhang et al 2022). To better resolve the chemical differences between lunar basalts and their sources, we normalize the Apollo high-Ti basalt and high-K KREEP and the CE-5 basalt to the Apollo low-Ti basalt which eliminates some effects of differentiation of the lunar magma ocean (Fig. 6c). The CE-5 basalt shows a pattern of incompatible lithophile trace elements similar to high-K KREEP, with the typical depletion of K, Nb, Ta, Sr, P, Eu, and Ti relative to neighboring elements and a factor of 3 lower concentrations only. Moreover, the Nb/Ta and Zr/Hf ratios of the CE-5 basalts are similar to the KREEP-related samples but higher than low-Ti and high-Ti basalts (Fig. 8).

Based on Sr-Nd isotopic compositions, Tian et al. (2021) suggest that the CE-5 basalts were derived from a non-KREEP mantle source and the KREEP-like signature resulted from low-degree partial melting followed by very high-degree fractional crystallization. Such a model was mainly suggested to explain the pattern and high concentrations of REE. However, our new bulk-rock data include a wider range of trace elements and are difficult to reconcile with the melting and fractionation model proposed by Tian et al. (2021). For example, given the rather low partition coefficients (0.0001–0.065) (Adam and Green, 2006; Bonechi et al., 2021; Dygert et al., 2020; Klemme et al., 2006; McKenzie and O'nions, 1991), the highly incompatible elements K, Th, U, Nb, and Ta are hardly incorporated into the typical phases such as olivine, orthopyroxene, and clinopyroxene. Therefore, partial melting and crystallization would mainly elevate their concentrations but not change the patterns or ratios of these elements. Fig. 6c shows specific fractionations of Ti, Nb, and Ta relative to Th, U, and the LREE that are "endemic" to the KREEP component in the Moon. The Nb/Ta ratio in the CE-5 basalts (Fig. 8) is also similar to KREEP basalts and unlike Nb/Ta in low- and high-Ti mare basalts. These features cannot be explained by the magmatic differentiation of common silicate minerals. According to our model presented in Fig. 9, partial melting of a non-KREEP mantle cumulate (olivine + pyroxene) of lunar magma ocean at low degrees (e.g., 3%) and the subsequence of fractional crystallization at variable degrees (20–50%) can significantly increase the concentrations of incompatible elements but their patterns hardly change and these processes would not fractionate high-field strength elements from neighbor elements. Warren and Wasson (1979) have highlighted the rather similar trace element patterns for all KREEPy samples from the Apollo landing sites, irrespective of the proportions of KREEP components. Therefore, we suggest that the KREEP-like trace element pattern of the CE-5 basalts was inherited from a KREEP-bearing mantle source. However, the proportion of high-K KREEP is not >2% (Fig. 9a-b) in the mantle source to reconcile with the unradiogenic Sr and radiogenic Nd isotope compositions of the CE-5 basalts as discussed below.

4.4. Clinopyroxene-rich mantle source for the origin of the CE-5 basalts

KREEP-bearing mantle sources are typically characterized by the evolved Sr-Nd isotopic compositions due to the high Rb/Sr and low Sm/Nd ratios of the KREEP (Borg et al., 2004; Snyder et al., 2000). Tian et al. (2021) thus proposed that the low initial ^{87}-

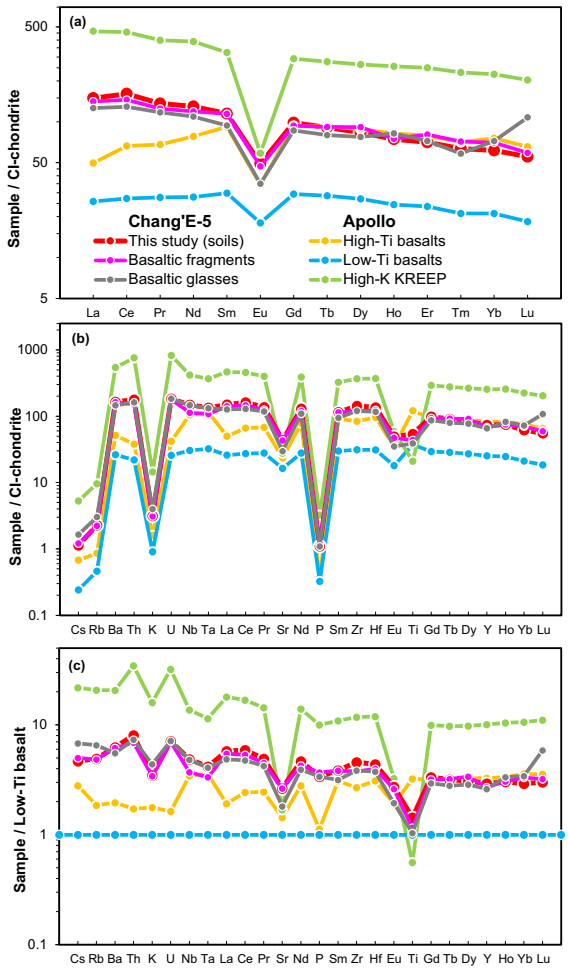

Fig. 6. (a-b) CI-chondrite normalized REE and multiple-element patterns of the CE-5 soils in this study and comparison with the CE-5 basaltic glasses and fragments from He et al. (2022). (c) Low-Ti basalt normalized multiple-element patterns of the CE-5 soils in this study and basaltic glasses and fragments from He et al. (2022). Note that the high concentrations of incompatible trace elements (e.g., Ba, Th, U, Nb, Ta, Zr, Hf, and REE) of the CE-5 soils are the same as the results of the CE-5 basaltic glasses and fragments. The trace element pattern of the CE-5 basalt/soil mimics the high-K KREEP. The CI-chondrite values are from McDonough and Sun (1995). The data of lunar low-Ti (Apollo 12&15) and high-Ti (Apollo 11&17) basalts are from The Lunar Sample Compendium (https://www-curator.jsc.nasa.gov/lunar/lsc/index.cfm) and only ICP-MS data are used here. The values of the high-K KREEP are from Warren (1989).

$Sr/^{86}Sr$ ratios (0.69934–0.69986) and positive ε_{Nd}(2.0 Ga) values (7.9–9.3) reflect a non-KREEP mantle source of the CE-5 basalts. We note that Rb/Sr and Sm/Nd ratios of the mantle sources are controlled by their mineral assemblages. Beard et al. (1998) have shown that the systematic Hf-Nd isotopic difference between the low-Ti and high-Ti basalts is a result of time-integrated differences in their mantle sources. Many high-Ti and low-Ti basalts display initial unradiogenic Sr and radiogenic Nd isotopes, and the compositions reflect variable proportions of olivine, orthopyroxene, and clinopyroxene in the mantle sources (Snyder et al., 2000). The CE-5 basalts display no fractionation of medium REE from heavy REE (Fig. 6a), indicating its origin from garnet-free, shallow magma ocean cumulates (Neal, 2001; Snyder et al., 1992). Clinopyroxene-bearing mineral assemblages were proposed to represent the typical late-stage cumulate during the solidification of the lunar magma ocean (Elkins-Tanton et al., 2011; Lin et al., 2017; Snyder et al., 1992). Relative to olivine and orthopyroxene, clinopyroxene contains more REE and Sr in the mantle and has high D_{Sm}/D_{Nd} and low D_{Rb}/D_{Sr} values of 1.3–2.1 (Bonechi et al., 2021) and 0.02–0.16 (McKenzie and O'nions, 1991; Vannucci et al., 1998), respectively, which are complementary to the low Sm/Nd and high Rb/Sr signatures of KREEP.

Numerous experimental and numerical studies have been carried out on the crystallization of the lunar magma ocean (LMO) (e.g., Elkins-Tanton et al., 2011; Lin et al., 2017, 2020; Rapp and Draper, 2018; Snyder et al., 1992). They consistently show the predominant crystallization of olivine and orthopyroxene before the crystallized percent solid (CPS) at 78% (78 CPS). However, the proportion of clinopyroxene is varied from 17% to 60% after ~ 80% solidification of LMO. In our model, we thus follow the proposed early crystallization sequence of the LMO by Snyder et al. (1992) and suggest that the LMO firstly experienced 40% and 38% equilibrium crystallization of olivine and orthopyroxene at CPS of 40% and 78% (40 CPS and 78 CPS) of LMO, respectively. Then we suggest that the remaining LMO experienced 8% fractional crystallization with varied clinopyroxene and olivine proportions, which is composed of plagioclase (50%), olivine (35–0%) + clinopyroxene (0–35 %) + pigeonite (10%) and orthopyroxene (5%) at 86 CPS of LMO. Because the crystalized plagioclase would float to the LMO surface and form the initial lunar anorthite crust, the upper mantle cumulate of the 86 CPS consists of olivine (70–0%) + clinopyroxene (0–70%) + pigeonite (20%) + orthopyroxene (10%). In our model, the total proportions of olivine and clinopyroxene are assumed to be 70% and the proportion of clinopyroxene thus can be adjusted from 0% to 70% to reconcile with $^{147}Sm/^{144}Nd$ and $^{87}Rb/^{86}Sr$ ratios in the KREEP-bearing mantle sources and trace element patterns of the CE-5 basalt as illustrated in Fig. 9. The details of the modeling method and results can be found in the Supplementary Material. Such 86 CPS with a few percent of high-K KREEP is considered as the mantle source of the CE-5 basalts.

As Fig. 9a-b shows, 0.3%, 0.5%, 1%, and 1.5% high-K KREEP components would require 10%, 20%, 40%, and 60% clinopyroxenes in the 86 CPS (A, B, C, and D cases in Fig. 9a-b), respectively, to produce the mantle source Sr-Nd isotopic compositions of the CE-5 basalts ($^{147}Sm/^{144}Nd$ = 0.222–0.227 and $^{87}Rb/^{86}Sr$ = 0.009–0.022) calculated by Tian et al. (2021). Importantly, partial melting of such clinopyroxene and KREEP-bearing mantle source (A, B, C, and D cases in Fig. 9a-b) at low degrees (e.g., 3%) of melting and subsequent fractional crystallization (e.g., 20–50%) could produce a melt with the KREEP-like pattern similar to the CE-5 basalts (Fig. 9c-f, see Supplementary Material for details). In these models, trace element contents of melts derived from the 86 CPS mantle source with high proportions of clinopyroxene (40–60%) and high-K KREEP (1–1.5%) are more consistent with the CE-5 basalts (Fig. 9e-f) relative to mantle source with low proportions of clinopyroxene (10–20%) and high-K KREEP (0.3–0.5%) (Fig. 9c-d). For the mantle source of the CE-5 basalt, a higher proportion of clinopyroxene is required to balance an increasing amount of KREEP. However, if the proportion of high-K KREEP exceeds 2% in the 86 CPS, the required high proportion of clinopyroxene (>70%) cannot meet $^{147}Sm/^{144}Nd$ and $^{87}Rb/^{86}Sr$ ratios for the CE-5 basaltic mantle source (Fig. 9a, b). A slightly higher μ-value ($^{238}U/^{204}Pb$) of ~ 680 in the CE-5 basalt mantle source (Che et al., 2021; Li et al., 2021b), compared to low-Ti basalts (~410–650) but different from high-Ti basalts (~360–390) (Snape et al., 2019), is also consistent with the contribution of a small amount (<2%) of KREEP component in the origin of the CE-5 basalts (Che et al., 2021).

Therefore, we suggest that the mantle source of the CE-5 basalts formed from late-stage cumulates of the crystallization of the lunar magma ocean, which were very likely to be characterized by high proportions of clinopyroxene (40–60%) cumulates with a small fraction (1–1.5%) of KREEP-like material. The KREEP-like materials may be equivalent to the former trapped interstitial liquid in the lunar upper mantle as suggested before (Snyder et al., 2000;

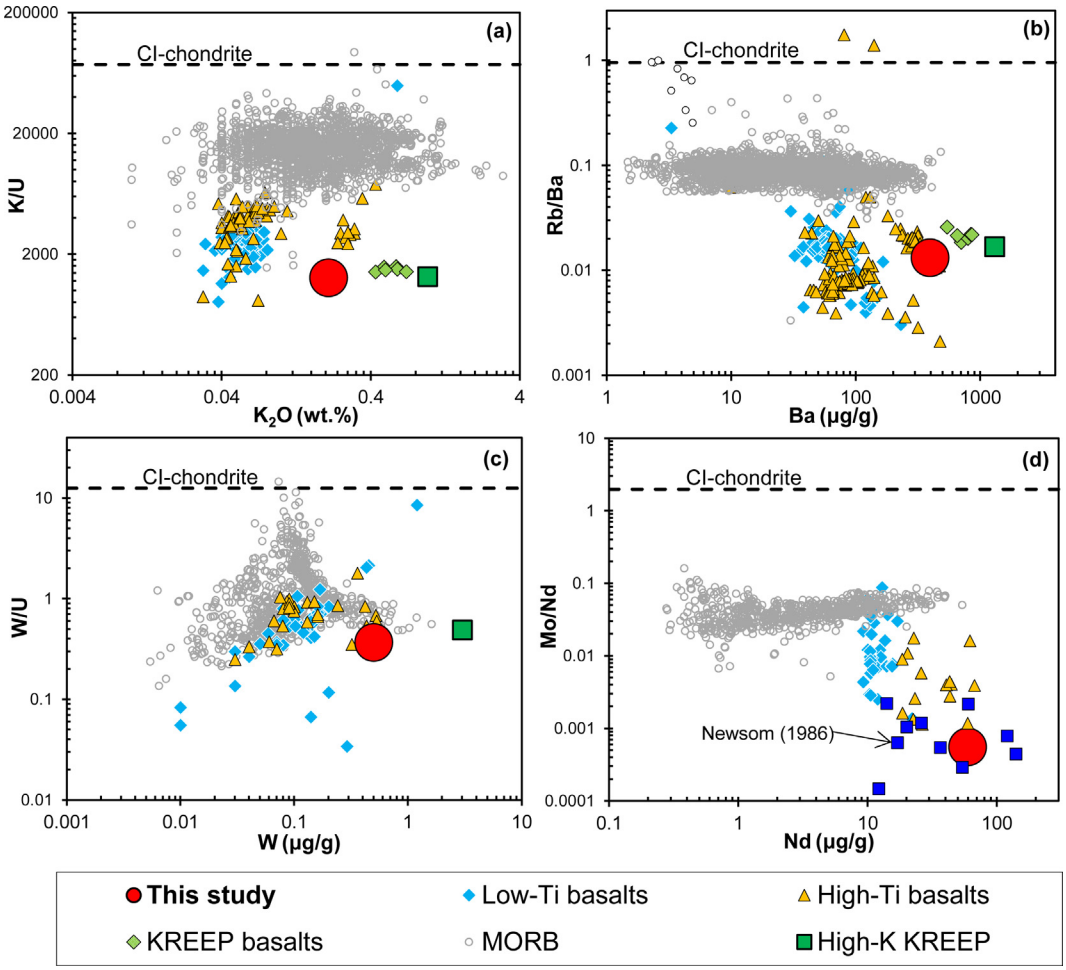

Fig. 7. (a) K/U versus K_2O, (b) Rb/Ba versus Ba, (c) W/U versus W, and (d) Mo/Nd versus Nd of the CE-5 soils. The depletion extents of volatile (K and Rb) and siderophile (W and Mo) elements in their mantle sources are comparable for the CE-5 basalts and lunar samples returned by the Apollo and Luna missions. The lunar low-Ti (Apollo 12&15), high-Ti (Apollo 11&17), and KREEP basalts (Apollo 14&15) are from The Lunar Sample Compendium (https://www-curator.jsc.nasa.gov/lunar/lsc/index.cfm). High-quality Mo data from Newsom (1986) are highlighted in Fig. 7d. The values of the high-K KREEP are from Warren (1989). The data of terrestrial mid-ocean ridge basalts (MORB) are from Gale et al. (2013).

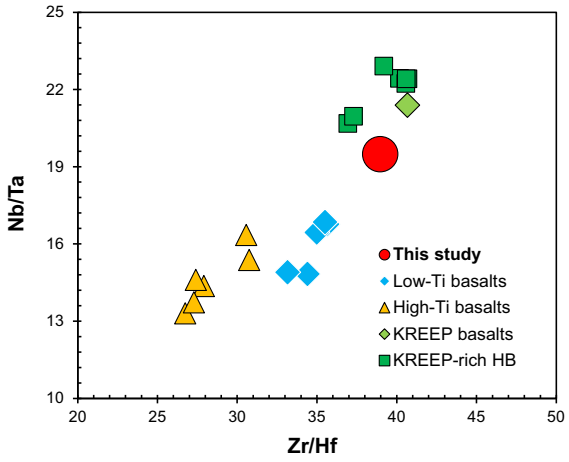

Fig. 8. Plot of Nb/Ta versus Zr/Hf of the CE-5 soils. High-precision data obtained by isotope dilution of the low-Ti, high-Ti, and KREEP basalts and KREEP-rich highland breccias (HB) are from Münker (2010) and references therein.

Snyder et al., 1992). Given the low liquidus temperatures of the late crystallized phases (Elkins-Tanton et al., 2011; Lin et al., 2017; Snyder et al., 1992), such a clinopyroxene-rich (relative to olivine and orthopyroxene) shallow mantle source with a slightly enhanced inventory of radioactive elements could preferentially melt relative to more incompatible element-depleted deeper lunar mantle cumulates and thus may potentially explain the prolonged lunar basaltic magmatism until 2.0 Ga.

5. Conclusions

Concentrations of 48 major and trace elements of two batches of the Chang'E-5 (CE-5) lunar soils have been simultaneously obtained by ICP-MS from the same sample aliquots. The soil predominantly comprises local mare basalts with negligible contamination (<5%) by highland and KREEP materials. About 1% of meteoritic materials were added via micrometeorite impacts and occasional agglutinates likely are unevenly distributed in the CE-5 soils. The CE-5 lunar soil is very fine (95% of the CE-5 soil by mass is distributed in the size of 4.84–432.3 μm, Li et al., 2022) and predominantly derived from the local mare basalt, likely leading to its uniform chemical composition even at the 2 mg sampling level (except for Ni). Except for some siderophile elements such as Ni and Ir, the bulk chemical composition of the CE-5 soil mostly represents the composition of local basalt.

The laboratory-based compositions of the CE-5 lunar soil overall confirm the TiO_2, Th, and FeO concentrations estimated from

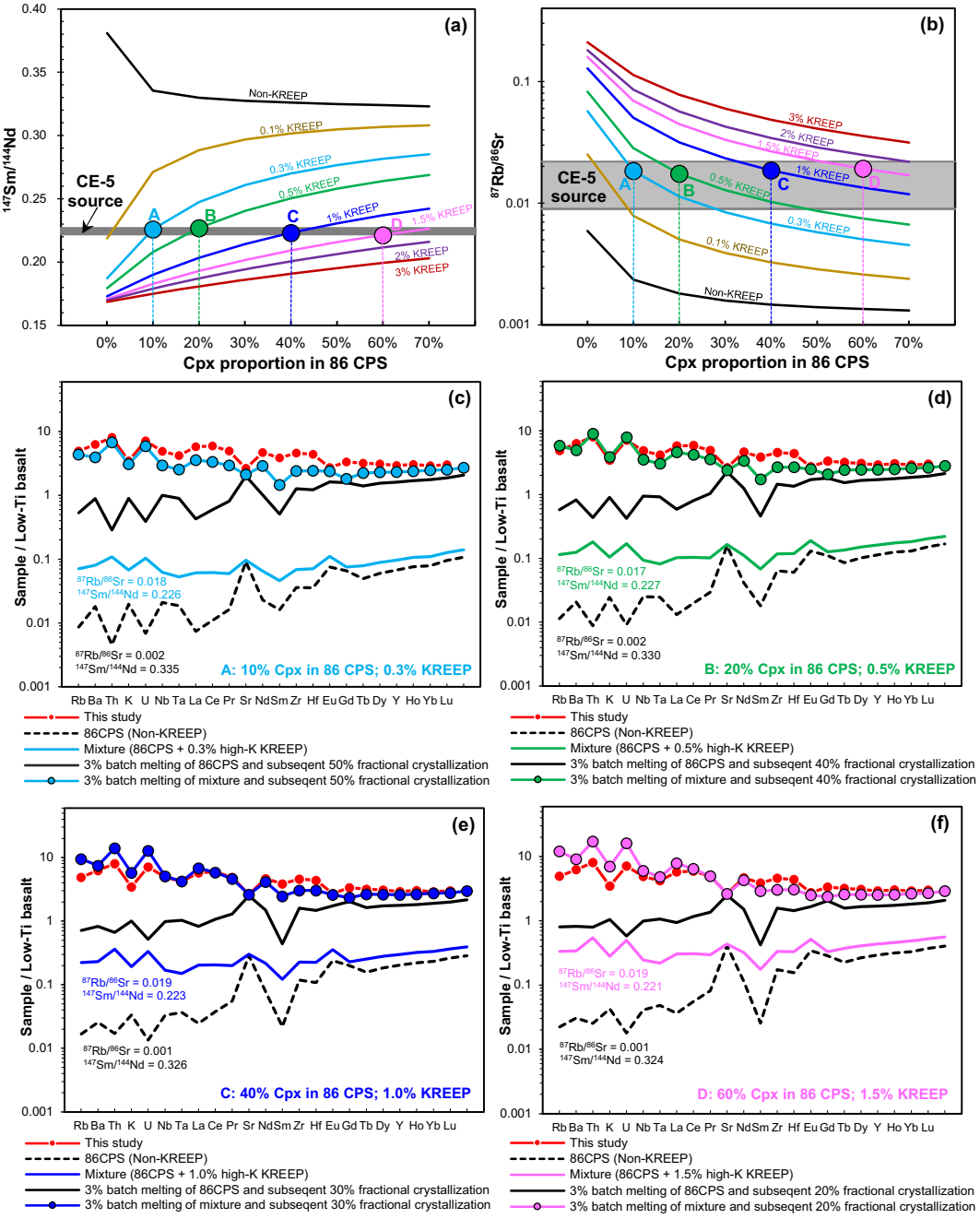

Fig. 9. Modeling results explaining KREEP-like trace elements and Sr-Nd isotopes of the CE-5 basalts. (a-b) Variable proportions of clinopyroxene (0–70%) and high-K KREEP (0–3%) in the mantle sources are calculated to reconcile with $^{147}Sm/^{144}Nd$ and $^{87}Rb/^{86}Sr$ ratios in the mantle sources of the CE-5 basalt. According to the crystallization sequence of the lunar magma ocean (LMO) proposed by Snyder et al. (1992), we assume the upper mantle cumulate of LMO at a crystallized percent solid (CPS) of 86% (86 CPS) is composed of olivine (Ol), orthopyroxene (Opx), clinopyroxene (Cpx), and pigeonite (Pig). The total weight of Ol and Cpx is fixed as 70% and the rest 30% of minerals are composed of 20% Pig and 10% Opx in the 86CPS. The proportion of Cpx in the 86 CPS varies from 0% to 70% (a-b). The marked A, B, C, and D in Fig. 9a-b are the cases that show KREEP (0.3–1.5%)-bearing mantle sources can produce the same $^{147}Sm/^{144}Nd$ and $^{87}Rb/^{86}Sr$ ratios as the mantle sources of the CE-5 basalt. The recommended $^{147}Sm/^{144}Nd$ and $^{87}Rb/^{86}Sr$ ranges of the mantle source of the CE-5 basalts are cited from Tian et al. (2021). The values of the high-K KREEP are from Warren (1989). The detailed original compositions of LMO, partition coefficients of minerals, modeling processes, and calculated results of 86 CPS with variable proportions of Cpx (0–70%) are listed in Tables S4-S7 and the modeling method in the Supplementary Material. (c-f) The A, B, C, and D cases in Fig. 9a-b are further illustrated to match trace element compositions of the CE-5 basalts. The 3% batch melting of these mixtures, which are composed by 0.3–1.5% high-K KREEP and 86 CPS with 10–60% Cpx, and subsequent 20–50% fractional crystallization (40% Cpx + 25% Pl + 20% Ol + 10% Pig + 5% Opx) can produce a melt with the KREEP-like pattern similar to the CE-5 basalts. The detailed modeling processes and calculated results are shown in the modeling method and Table S8, respectively, in the Supplementary Material. The data of lunar low-Ti (Apollo 12&15) basalt are from The Lunar Sample Compendium (https://www-curator.jsc.nasa.gov/lunar/lsc/index.cfm) and only ICP-MS data are used here.

remote sensing approaches, supporting the widespread distribution of intermediate-Ti, high-FeO, and high-Th basalts in the Procellarum-KREEP Terrain. Chemically, the CE-5 soil is distinct from basalts and soils returned by the Apollo and Luna missions, however, the depletion extents of volatile and siderophile elements in their mantle sources inferred from suitable element ratios such as K/U, Rb/Ba, W/U, and Mo/Nd are comparable. The CE-5 basalt that is represented by the soil belongs to intermediate Ti and low-K lunar basalt types with notably high FeO concentration and low Mg# (34). Importantly, the CE-5 basalt displays KREEP-

rich trace element compositions, e.g., notable enrichment of REE, Th, and other incompatible elements, and the relative ratios (e.g., Nb/Ta and Zr/Hf) of these elements cannot be explained by partial melting and crystallization of a non-KREEP mantle source. Instead, the KREEP-like trace element patterns must have resulted from the KREEP-bearing mantle source of the CE-5 basalts, which is different from the non-KREEP mantle source model proposed by Tian et al (2021). Therefore, the CE-5 basalt likely originated from a shallow mantle source that consists of a high proportion of clinopyroxene relative to olivine and orthopyroxene with a small fraction (1–1.5%) of KREEP-like material, which could explain both trace element patterns and unradiogenic Sr and radiogenic Nd isotope compositions.

Declaration of Competing Interest

The authors declare that they have no known competing financial interests or personal relationships that could have appeared to influence the work reported in this paper.

Acknowledgements

We appreciate all staff of the Chang'E-5 mission and their great effort makes this work possible. We thank the China National Space Administration Agency for providing access to the Chang'E-5 returned samples CE5C0400 and CE5C0600. Randy L. Korotev, Marc D. Norman, and two anonymous reviewers are thanked for providing the detailed reviews and great suggestions. We thank Marc D. Norman for editorial handling. We thank Haihong Chen, Ming Li, and Shuo Liu for their kind support in the clean laboratory. We also thank Yuanyang Yu, Feng Liu, Yu Yuan, Ting Qu, Yang Gao, and Ran Lin for compiling data of Apollo and Luna samples and lunar meteorites. This work was supported by the pre-research project on Civil Aerospace Technologies funded by China National Space Administration Agency (Grant No. D020205), the National Natural Science Foundation of China (Grant No. 41922021), and the MOST Special Fund from the State Key Laboratory of Geological Processes and Mineral Resources, China University of Geosciences (Grant No. MSFGPMR01-03; MSFGPMR10).

Appendix A. Supplementary material

Supplementary material to this article can be found online at https://doi.org/10.1016/j.gca.2022.06.037.

References

Adam, J., Green, T., 2006. Trace element partitioning between mica- and amphibole-bearing garnet lherzolite and hydrous basanitic melt: 1. Experimental results and the investigation of controls on partitioning behaviour. Contrib. Mineral. Petrol. 152, 1–17.

Albarede, F., Albalat, E., Lee, C.T.A., 2015. An intrinsic volatility scale relevant to the Earth and Moon and the status of water in the Moon. Meteorit. Planet. Sci. 50, 568–577.

Ammann, A.A., 2007. Inductively coupled plasma mass spectrometry (ICP MS): a versatile tool. J. Mass Spectrom. 42, 419–427.

Anders, E., Ganapathy, R., Krähenbühl, U., Morgan, J.W., 1973. Meteoritic material on the moon. The moon, 3–24.

Beard, B.L., Taylor, L.A., Scherer, E.E., Johnson, C.M., Snyder, G.A., 1998. The Source Region and Melting Mineralogy of High-Titanium and Low-Titanium Lunar Basalts Deduced from Lu-Hf Isotope Data. Geochim. Cosmochim. Acta 62, 525–544.

Bonechi, B., Perinelli, C., Gaeta, M., Fabbrizio, A., Petrelli, M., Strnad, L., 2021. High pressure trace element partitioning between clinopyroxene and alkali basaltic melts. Geochim. Cosmochim. Acta 305, 282–305.

Borg, L.E., Shearer, C.K., Asmerom, Y., Papike, J.J., 2004. Prolonged KREEP magmatism on the Moon indicated by the youngest dated lunar igneous rock. Nature 432, 209–211.

Bottke, W.F., Norman, M.D., 2017. The Late Heavy Bombardment. Annu. Rev. Earth Planet. Sci. 45, 619–647.

Cao, K., Dong, M., She, Z., Xiao, Q, Wang, X., Qian, Y., Li, Y., Wang, Z., He, Q., Wu, X., Zong, K., Hu, Z., Xiao, L., 2022. A novel method for simultaneous analysis of particle size and mineralogy for Chang'E-5 lunar soil with minimum sample consumption. Sci. China-Earth Sci. https://doi.org/10.1007/s11430-022-9966-5.

Che, X., Nemchin, A., Liu, D., Long, T., Wang, C., Norman, M.D., Joy, K.H., Tartese, R., Head, J., Jolliff, B., Snape, J.F., Neal, C.R., Whitehouse, M.J., Crow, C., Benedix, G., Jourdan, F., Yang, Z., Yang, C., Liu, J., Xie, S., Bao, Z., Fan, R., Li, D., Li, Z., Webb, S.G., 2021. Age and composition of young basalts on the Moon, measured from samples returned by Chang'e-5. Science 374, 887–890.

Dygert, N., Draper, D.S., Rapp, J.F., Lapen, T.J., Fagan, A.L., Neal, C.R., 2020. Experimental determinations of trace element partitioning between plagioclase, pigeonite, olivine, and lunar basaltic melts and an fO2 dependent model for plagioclase-melt Eu partitioning. Geochim. Cosmochim. Acta 279, 258–280.

Day, J.M.D., 2020. Metal grains in lunar rocks as indicators of igneous and impact processes. Meteorit. Planet. Sci. 55, 1793–1807.

Day, J.M.D., Pearson, D.G., Taylor, L.A., 2007. Highly Siderophile Element Constraints on Accretion and Differentiation of the Earth-Moon System. Science 315, 217–219.

Elkins-Tanton, L.T., Burgess, S., Yin, Q.-Z., 2011. The lunar magma ocean: Reconciling the solidification process with lunar petrology and geochronology. Earth Planet. Sci. Lett. 304, 326–336.

Fischer-Gödde, M., Becker, H., 2012. Osmium isotope and highly siderophile element constraints on ages and nature of meteoritic components in ancient lunar impact rocks. Geochim. Cosmochim. Acta 77, 135–156.

Fu, X., Hou, X., Zhang, J., Li, B., Ling, Z., Jolliff, B.L., Xu, L., Zou, Y., 2021. Possible Non-Mare Lithologies in the Regolith at the Chang'E-5 Landing Site: Evidence From Remote Sensing Data. J. Geophys. Res.: Planets 126. e2020JE006797.

Gale, A., Dalton, C.A., Langmuir, C.H., Su, Y.J., Schilling, J.-G., 2013. The mean composition of ocean ridge basalts. *Geochem., Geophys.* Geosyst. 14, 489–518.

Giguere, T.A., Taylor, G.J., Hawke, B.R., Lucey, P.G., 2000. The titanium contents of lunar mare basalts. Meteorit. Planet. Sci. 35, 193–200.

Gillis, J.J., Jolliff, B.L., Elphic, R.C., 2003. A revised algorithm for calculating TiO_2 from Clementine UVVIS data: A synthesis of rock, soil, and remotely sensed TiO_2 concentrations. J. Geophys. Res.: Planets 108, 5009.

Gillis, J.J., Jolliff, B.L., Korotev, R.L., 2004. Lunar surface geochemistry: Global concentrations of Th, K, and FeO as derived from lunar prospector and Clementine data. Geochim. Cosmochim. Acta 68, 3791–3805.

Ganapathy, R., Keays, R.R., Anders, E., 1970. Apollo 12 Lunar Samples: Trace Element Analysis of a Core and the Uniformity of the Regolith. Science 170, 533–535.

Haskin, L., Warren, P., 1991. Lunar Chemistry. In: Heiken, G.H., Vaniman, D.T., French, B.M. (Eds.), Lunar Sourcebook: A User's Guide to the Moon. Cambridge University Press, Cambridge, UK, pp. 357–474.

He, Q., Li, Y., Baziotis, I., Qian, Y., Xiao, L., Wang, Z., Zhang, W., Luo, B., Neal, C.R., Day, J.M.D., Pan, F., She, Z., Wu, X., Hu, Z., Zong, K., Wang, L., 2022. Detailed petrogenesis of the unsampled Oceanus Procellarum: The case of the Chang'e-5 mare basalts. Icarus 383, 115082.

Head, J.W., Wilson, L., 2020. Rethinking Lunar Mare Basalt Regolith Formation: New Concepts of Lava Flow Protolith and Evolution of Regolith Thickness and Internal Structure. Geophys. Res. Lett. 47. e2020GL088334.

Hiesinger, H., Head, J., Wolf, U., Jaumann, R., Neukum, G., 2011. Ages and stratigraphy of lunar mare basalts: A synthesis. In: Ambrose, W.A., Williams, D.A. (Eds.), Recent advance and current research issues in Lunar stratigraphy: *Spec. Pap. - Geol. Soc. Am.*, pp. 1–51.

Hiesinger, H., Head III, J.W., 2006. New Views of Lunar Geoscience: An Introduction and Overview. Rev. *Mineral. Geochem.* 60, 1–81.

Hu, S., He, H., Ji, J., Lin, Y., Hui, H., Anand, M., Tartèse, R., Yan, Y., Hao, J., Li, R., Gu, L., Guo, Q., He, H., Ouyang, Z., 2021. A dry lunar mantle reservoir for young mare basalts of Chang'e-5. Nature 600, 49–53.

Jolliff, B.L., Gillis, J.J., Haskin, L.A., Korotev, R.L., Wieczorek, M.A., 2000. Major lunar crustal terranes: Surface expressions and crust-mantle origins. J. Geophys. Res.: Planets 105, 4197–4216.

Keays, R.R., Ganapathy, R., Laul, J.C., Anders, E., Herzog, G.F., Jeffery, P.M., 1970. Trace Elements and Radioactivity in Lunar Rocks: Implications for Meteorite Infall, Solar-Wind Flux, and Formation Conditions of Moon. Science 167, 490–493.

Klemme, S., Günther, D., Hametner, K., Prowatke, S., Zack, T., 2006. The partitioning of trace elements between ilmenite, ulvospinel, armalcolite and silicate melts with implications for the early differentiation of the moon. Chem. Geol. 234, 251–263.

Korotev, R.L., Gillis, J.J., 2001. A new look at the Apollo 11 regolith and KREEP. J. Geophys. Res.: Planets 106, 12339–12353.

Korotev, R.L., Jolliff, B.L., Zeigler, R.A., Seddio, S.M., Haskin, L.A., 2011. Apollo 12 revisited. Geochim. Cosmochim. Acta 75, 1540–1573.

Laneuville, M., Taylor, J., Wieczorek, M., 2018. Distribution of Radioactive Heat Sources and Thermal History of the Moon. J. Geophys. Res.: Planets 123, 3144–3166.

Lawrence, D.J., Feldman, W.C., Barraclough, B.L., Binder, A.B., Elphic, R.C., Maurice, S., Thomsen, D.R., 1998. Global elemental maps of the Moon: The Lunar Prospector gamma-ray spectrometer. Science 281, 1484–1489.

Lawrence, D.J., Feldman, W.C., Elphic, R.C., Little, R.C., Prettyman, T.H., Maurice, S., Lucey, P.G., Binder, A.B., 2002. Iron abundances on the lunar surface as measured by the Lunar Prospector gamma-ray and neutron spectrometers. J. Geophys. Res.: Planets 107, 13-1-13-26.

Li, C., Hu, H., Yang, M.-F., Pei, Z.-Y., Zhou, Q., Ren, X., Liu, B., Liu, D., Zeng, X., Zhang, G., Zhang, H., Liu, J., Wang, Q., Deng, X., Xiao, C., Yao, Y., Xue, D., Zuo, W., Su, Y.,

Wen, Ouyang, Z., . Characteristics of the lunar samples returned by Chang'E-5 mission. Natl. Sci. Rev. 9. nwab188.
Li, J.W., Zong, K.Q., He, Q., Wang, Z.C., Hu, Z.C., 2021a. Accurate determination of major and trace elements of lunar soil simulant by ICPMS. Journal of Nanjing University (Natural Science) 57, 944–956.
Li, Q.-L., Zhou, Q., Liu, Y., Xiao, Z., Lin, Y., Li, J.-H., Ma, H.-X., Tang, G.-Q., Guo, S., Tang, X., Yuan, J.-Y., Li, J., Wu, F.-Y., Ouyang, Z., Li, C., Li, X.-H., 2021b. Two billion-year-old volcanism on the Moon from Chang'E-5 basalts. Nature 600, 54–58.
Lin, Y., Hui, H., Xia, X., Shang, S., van Westrenen, W., 2020. Experimental constraints on the solidification of a hydrous lunar magma ocean. Meteorit. Planet. Sci. 55, 207–230.
Lin, Y., Tronche, E.J., Steenstra, E.S., van Westrenen, W., 2017. Evidence for an early wet Moon from experimental crystallization of the lunar magma ocean. Nature Geosci. 10, 14–18.
Liu, T., Michael, G., Zhu, M.-H., Wünnemann, K., 2021. Predicted Sources of Samples Returned From Chang'e−5 Landing Region. Geophys. Res. Lett. 48. e2021GL092434.
Liu, Y.S., Gao, S., Hu, Z.C., Gao, C.G., Zong, K.Q., Wang, D.B., 2010. Continental and oceanic crust recycling-induced melt-peridotite interactions in the Trans-North China Orogen: U-Pb dating, Hf isotopes and trace elements in zircons from mantle xenoliths. J. Petrol. 51, 537–571.
Longerich, H.P., Jenner, G.A., Fryer, B.J., Jackson, S.E., 1990. Inductively coupled plasma-mass spectrometric analysis of geological samples: A critical evaluation based on case studies. Chem. Geol. 83, 105–118.
McDonough, W.F., Sun, S.S., 1995. The composition of the Earth. Chem. Geol. 120, 223–253.
McKay, D.S., Heiken, G., Basu, A., Blanford, G., Simon, S., Reedy, R., French, B.M., Papike, J., 1991. The Lunar Regolith. In: Heiken, G.H., Vaniman, D.T., French, B.M. (Eds.), Lunar Sourcebook: A User's Guide to the Moon. Cambridge University Press, Cambridge, UK, pp. 285–356.
McKay, D.S., Fruland, R.M., Heiken, G.H., 1974. Grain size and the evolution of lunar soil. In: Proceedings 5th Lunar Science Conference, pp. 887–906.
McKenzie, D., O'nions, R., 1991. Partial melt distributions from inversion of rare earth element concentrations. J. Petrol. 32, 1021–1091.
Münker, C., 2010. A high field strength element perspective on early lunar differentiation. Geochim. Cosmochim. Acta 74, 7340–7361.
Neal, C.R., 2001. Interior of the Moon: The presence of garnet in the primitive deep lunar mantle. J. Geophys. Res.: Planets 106, 27865–27885.
Neal, C.R., Taylor, L.A., 1992. Petrogenesis of mare basalts: A record of lunar volcanism. Geochim. Cosmochim. Acta 56, 2177–2211.
Newsom, H.E., 1986. Constraints on the origin of the Moon from the abundance of molybdenum and other siderophile elements. In: Hartmann, W.K., Phillips, R.J., Taylor, G.J. (Eds.), Origin of the Earth and Moon. University of Arizona Press, Tucson, AZ, pp. 203–229.
Norman, M.D., Bennett, V.C., Ryder, G., 2002. Targeting the impactors: siderophile element signatures of lunar impact melts from Serenitatis. Earth Planet. Sci. Lett. 202, 217–228.
Prettyman, T.H., Hagerty, J.J., Elphic, R.C., Feldman, W.C., Lawrence, D.J., McKinney, G.W., Vaniman, D.T., 2006. Elemental composition of the lunar surface: Analysis of gamma ray spectroscopy data from Lunar Prospector. J. Geophys. Res.: Planets 111, E12007.
Qian, Y., Xiao, L., Head, J.W., van der Bogert, C.H., Hiesinger, H., Wilson, L., 2021a. Young lunar mare basalts in the Chang'e-5 sample return region, northern Oceanus Procellarum. Earth Planet. Sci. Lett. 555, 116702.
Qian, Y., Xiao, L., Wang, Q., Head, J.W., Yang, R., Kang, Y., van der Bogert, C.H., Hiesinger, H., Lai, X., Wang, G., Pang, Y., Zhang, N., Yuan, Y., He, Q., Huang, J., Zhao, Wang, J., Zhao, S., 2021b. China's Chang'e-5 landing site: Geology, stratigraphy, and provenance of materials. Earth Planet. Sci. Lett. 561, 116855.
Rapp, J.F., Draper, D.S., 2018. Fractional crystallization of the lunar magma ocean: Updating the dominant paradigm. Meteorit. Planet. Sci. 53, 1432–1455.
Scott, E.R.D., Wasson, J.T., 1975. Classification and properties of iron meteorites. Rev. Geophys. 13, 527–546.
Shearer, C.K., Borg, L.E., 2006. Big returns on small samples: Lessons learned from the analysis of small lunar samples and implications for the future scientific exploration of the Moon. Geochemistry 66, 163–185.
Shearer, C.K., Hess, P.C., Wieczorek, M.A., Pritchard, M.E., Parmentier, E.M., Borg, L.E., Longhi, J., Elkins-Tanton, L.T., Neal, C.R., Antonenko, I., Canup, R.M., Halliday, A. N., Grove, T.L., Hager, B.H., Lee, D.-C., Wiechert, U., 2006. Thermal and Magmatic Evolution of the Moon. Rev. Mineral. Geochem. 60, 365–518.
Shearer, C.K., Papike, J.J., 1999. Magmatic evolution of the Moon. Am. Mineral. 84, 1469–1494.
Snape, J., Nemchin, A., Whitehouse, M., Merle, R., Hopkinson, T., Anand, M., 2019. The timing of basaltic volcanism at the Apollo landing sites. Geochim. Cosmochim. Acta 266, 29–53.
Snyder, G.A., Borg, L.E., Nyquist, L.E., Taylor, L.A., 2000. Chronology and isotopic constraints on lunar evolution. In: Canup, R.M., Righter, K. (Eds.), Origin of the Earth and Moon. University of Arizona Press, Tucson, AZ, pp. 361–396.
Snyder, G.A., Taylor, L.A., Neal, C.R., 1992. A chemical model for generating the sources of mare basalts: Combined equilibrium and fractional crystallization of the lunar magmasphere. Geochim. Cosmochim. Acta 56, 3809–3823.
Tian, H.-C., Wang, H., Chen, Y., Yang, W., Zhou, Q., Zhang, C., Lin, H.-L., Huang, C., Wu, S.-T., Jia, L.-H., Xu, L., Zhang, D., Li, X.-G., Chang, R., Yang, Y.-H., Xie, L.-W., Zhang, D.-P., Zhang, G.-L., Yang, S.-H., Wu, F.-Y., 2021. Non-KREEP origin for Chang'E-5 basalts in the Procellarum KREEP Terrane. Nature 600, 59–63.
Vannucci, R., Bottazzi, P., Wulff-Pedersen, E., Neumann, E.R., 1998. Partitioning of REE, Y, Sr, Zr and Ti between clinopyroxene and silicate melts in the mantle under La Palma (Canary Islands): implications for the nature of the metasomatic agents. Earth Planet. Sci. Lett. 158, 39–51.
Warren, P.H., 1985. The magma ocean concept and lunar evolution. Annu. Rev. Earth Planet. Sci. 13, 201–240.
Warren, P.H., 1989. KREEP: Major-Element Diversity, Trace-Element Uniformity (Almost). In: Taylor, G.J., Warren, P.H. (Eds.), Workshop on Moon in Transition: Apollo 14, KREEP, and Evolved Lunar Rocks. Lunar and Planetary Institute, Houston, Texas, pp. 149–153.
Warren, P.H., Wasson, J.T., 1979. The origin of KREEP. Rev. Geophys. 17, 73–88.
Wasson, J.T., Boynton, W.V., Chou, C.-L., Baedecker, P.A., 1975. Compositional evidence regarding the influx of interplanetary materials onto the lunar surface. The moon 13, 121–141.
Wasson, J.T., Kallemeyn, G.W., 1988. Compositions of Chondrites. Phil. Trans. R. Soc. **A** 325, 535–544.
Xie, M., Xiao, Z., Zhang, X., Xu, A., 2020. The Provenance of Regolith at the Chang'e-5 Candidate Landing Region. J. Geophys. Res.: Planets 125. e2019JE006112.
Yang, W., Lin, Y., 2021. New Lunar Samples Returned by Chang'e-5: Opportunities for New Discoveries and International Collaboration. Innovation 2, 100070.
Yao, Y., Xiao, C., Wang, P., Li, C., Zhou, Q., 2022. Instrumental Neutron Activation Analysis of Chang'E-5 Lunar Regolith Samples. J. Am. Chem. Soc. 144, 5478–5484.
Zhang, D., Su, B., Chen, Y., Yang, W., Mao, Q., Jia, L.-H., 2022. Titanium in olivine reveals low-Ti origin of the Chang'E-5 lunar basalts. Lithos 414–415, 106639.
Zhao, W., Zong, K., Liu, Y., Hu, Z., Chen, H., Li, M., 2019. An effective oxide interference correction on Sc and REE for routine analyses of geological samples by inductively coupled plasma-mass spectrometry. J. Earth Sci. 30, 1302–1310.